Photonic chip based tunable and reconfigurable narrowband microwave photonic filter using stimulated Brillouin scattering

Adam Byrnes,[1] Ravi Pant,[1] Enbang Li,[1] Duk-Yong Choi,[2] Christopher G. Poulton,[3] Shanhui Fan,[1,4] Steve Madden,[2] Barry Luther-Davies,[2] and Benjamin J. Eggleton[1,*]

[1]*Centre for Ultrahigh bandwidth Devices for Optical Systems (CUDOS), Institute of Photonics and Optical Science (IPOS), School of Physics, The University of Sydney, NSW 2006, Australia*
[2]*CUDOS, Laser Physics Centre, Australian National University, Canberra, ACT 0200, Australia*
[3]*CUDOS, University of Technology Sydney, Sydney, NSW 2007, Australia*
[4]*Department of Electrical Engineering, Stanford University, Stanford, California 94305, USA*
** egg@physics.usyd.edu.au*

Abstract: We report the first demonstration of a photonic chip based dynamically reconfigurable, widely tunable, narrow pass-band, high Q microwave photonic filter (MPF). We exploit stimulated Brillouin scattering (SBS) in a 6.5 cm long chalcogenide (As_2S_3) photonic chip to demonstrate a MPF that exhibited a high quality factor of ~520 and narrow bandwidth and was dynamically reconfigurable and widely tunable. It maintained a stable 3 dB bandwidth of 23 ± 2MHz and amplitude of 20 ± 2 dB over a large frequency tuning range of 2-12 GHz. By tailoring the pump spectrum, we reconfigured the 3 dB bandwidth of the MPF from ~20 MHz to ~40 MHz and tuned the shape factor from 3.5 to 2 resulting in a nearly flat-topped filter profile. This demonstration represents a significant advance in integrated microwave photonics with potential applications in on-chip microwave signal processing for RADAR and analogue communications.

OCIS codes: (190.2640) Stimulated scattering, modulation; (190.4390) Nonlinear optics, integrated optics; (060.5625) Radio frequency photonics.

References and links

1. J. Capmany, B. Ortega, and D. Pastor, "A tutorial on microwave photonic filters," J. Lightwave Technol. **24**(1), 201–229 (2006).
2. D. B. Hunter and R. A. Minasian, "Tunable microwave fiber-optic bandpass filters," IEEE Photon. Technol. Lett. **11**(7), 874–876 (1999).
3. Y. M. Chang and J. H. Lee, "High-Q tunable, photonic microwave single passband filter based on stimulated Brillouin scattering and fiber Bragg grating filtering," Opt. Commun. **281**(20), 5146–5150 (2008).
4. X. Yi and R. A. Minasian, "Microwave photonic filter with single bandpass response," Electron. Lett. **45**(7), 362–U31 (2009).
5. W. Li, M. Li, and J. Yao, "A narrow-passband and frequency-tunable microwave photonic filter based on phase-modulation to intensity-modulation conversion using a phase-shifted fiber Bragg grating," IEEE Trans. Microw. Theory Tech. **60**(5), 1287–1296 (2012).
6. M. Bolea, J. Mora, B. Ortega, and J. Capmany, "Highly chirped single-bandpass microwave photonic filter with reconfiguration capabilities," Opt. Express **19**(5), 4566–4576 (2011).
7. J. Mora, B. Ortega, A. Diez, J. L. Cruz, M. V. Andres, J. Capmany, and D. Pastor, "Photonic microwave tunable single-bandpass filter based on a Mach-Zehnder interferometer," J. Lightwave Technol. **24**(7), 2500–2509 (2006).
8. K. Zhu, H. Ou, H. Fu, E. Remb, and S. He, "A simple and tunable single-bandpass microwave photonic filter of adjustable shape," IEEE Photon. Technol. Lett. **20**(23), 1917–1919 (2008).
9. V. R. Supradeepa, C. M. Long, R. Wu, F. Ferdous, E. Hamidi, D. E. Leaird, and A. M. Weiner, "Comb-based radiofrequency photonic filters with rapid tunability and high selectivity," Nat. Photonics **6**(3), 186–194 (2012).
10. A. J. Torregrosa, H. Maestre, A. L. Recas, J. A. Pereda, J. Capmany, and C. R. Fernandez-Pousa, "Tunability of the multiple-bandpass response of cascaded single-source and continuous-sample microwave photonic filters," Opt. Commun. **283**(7), 1320–1325 (2010).

#170558 - $15.00 USD Received 13 Jun 2012; revised 23 Jul 2012; accepted 30 Jul 2012; published 1 Aug 2012

11. X. Xue, X. Zheng, H. Zhang, and B. Zhou, "Single-bandpass microwave photonic filter with wide tuning range and no baseband response," IEEE Photonics Conference 143–144 (2011).
12. J. Mora, J. Capmany, and L. R. Chen, "Tunable and reconfigurable single bandpass photonic microwave filter using a high-birefringence Sagnac loop and DVMM channel selector," IEEE Leos Annual Meeting **1-2**, 192–193 (2007).
13. B. Vidal, M. A. Piqueras, and J. Martí, "Tunable and reconfigurable photonic microwave filter based on stimulated Brillouin scattering," Opt. Lett. **32**(1), 23–25 (2007).
14. W. W. Zhang and R. A. Minasian, "Widely tunable single-passband microwave photonic filter based on stimulated Brillouin scattering," IEEE Photon. Technol. Lett. **23**(23), 1775–1777 (2011).
15. J. Sancho, Sanghoon Chin, M. Sagues, A. Loayssa, J. Lloret, I. Gasulla, S. Sales, L. Thévenaz, and J. Capmany, "Dynamic microwave photonic filter using separate carrier tuning based on stimulated Brillouin scattering in fibers," IEEE Photon. Technol. Lett. **22**(23), 1753–1755 (2010).
16. B. Vidal, T. Mengual, and J. Marti, "Photonic microwave filter with single bandpass response based on Brillouin processing and SSB-SC," International Topical Meeting on Microwave Photonics 92–95 (2009).
17. A. Loayssa, J. Capmany, M. Sagues, and J. Mora, "Demonstration of incoherent microwave photonic filters with all-optical complex coefficients," IEEE Photon. Technol. Lett. **18**(16), 1744–1746 (2006).
18. B. J. Eggleton, B. Luther-Davies, and K. Richardson, "Chalcogenide Photonics," Nat. Photonics **5**, 141–148 (2011).
19. B. J. Eggleton, T. D. Vo, R. Pant, J. Schr, M. D. Pelusi, D. Yong Choi, S. J. Madden, and B. Luther-Davies, "Photonic chip based ultrafast optical processing based on high nonlinearity dispersion engineered chalcogenide waveguids," Laser Photon. Rev. **6**(1), 97–114 (2012).
20. W. J. Chin, D. H. Kim, J. H. Song, and S. S. Lee, "Integrated photonic microwave bandpass filter incorporating a polymeric microring resonator," JJAP Part 1-Regular Papers Brief Communications & Review Papers **45**(4A), 2576–2579 (2006).
21. F. Coppinger, C. K. Madsen, and B. Jalali, "Photonic microwave filtering using coherently coupled integrated ring resonators," Microw. Opt. Technol. Lett. **21**(2), 90–93 (1999).
22. E. J. Norberg, R. S. Guzzon, J. S. Parker, L. A. Johansson, and L. A. Coldren, "Programmable photonic microwave filters monolithically integrated in InP-InGaAsP," J. Lightwave Technol. **29**(11), 1611–1619 (2011).
23. R. Pant, A. Byrnes, C. G. Poulton, E. Li, D.-Y. Choi, S. Madden, B. Luther-Davies, and B. J. Eggleton, "Photonic-chip-based tunable slow and fast light via stimulated Brillouin scattering," Opt. Lett. **37**(5), 969–971 (2012).
24. R. Pant, C. G. Poulton, D.-Y. Choi, H. Mcfarlane, S. Hile, E. Li, L. Thevenaz, B. Luther-Davies, S. J. Madden, and B. J. Eggleton, "On-chip stimulated Brillouin scattering," Opt. Express **19**(9), 8285–8290 (2011).
25. R. Pant, M. D. Stenner, M. A. Neifeld, Z. M. Shi, R. W. Boyd, and D. J. Gauthier, "Maximizing the opening of eye diagrams for slow-light systems," Appl. Opt. **46**(26), 6513–6519 (2007).

1. Introduction

Microwave filters form a critical part of microwave signal processing with applications in RADAR, radio over fiber (RoF), and mobile communications [1]. However, microwave filters implemented in the electrical domain suffer from electromagnetic interference (EMI), are difficult to tune and difficult to reconfigure in terms of the filter shape and its bandwidth [1]. Microwave *photonic* filters (MPFs), on the other hand, can provide a wide tuning range, are naturally immune to EMI, and some schemes exhibit the ability to be reconfigured [1]. In recent years, a number of MPF designs exhibiting either a periodic transfer function or a single pass-band have been demonstrated in optical fiber. These MPFs have been based on tapped delay lines and single pass-band architectures, realized using technologies such as Fiber Bragg Gratings (FBGs) [2–5]; Mach-Zehnder interferometers (MZIs) [6–8]; dispersion based tap delay [9, 10]; semiconductor optical amplifiers (SOAs) [11]; Sagnac loops [12]; or stimulated Brillouin scattering (SBS) [13–17].

When the MPF has a periodic transfer function, the tuning range is obviously limited by the free spectral range (FSR) and this also restricts the amount by which the bandwidth can be reconfigured. MPFs with a single pass-band are, therefore, better suited for applications where large tuning and large dynamic bandwidth are required [1]. Recently widely tunable single pass-band MPFs with high Q have been demonstrated by exploiting the narrow gain spectrum of SBS [13, 14, 16]. However, these impressive results were achieved in an optical fiber ~10-20 km long [13, 14, 16, 17] which makes them incompatible with all-optical integration [18, 19]. Quite impressive results have also been reported using chip-based photonic microwave signal processors, however, current MPF bandwidths have been limited to > 1 GHz and a Q factor of ~10 [20–22].

#170558 - $15.00 USD Received 13 Jun 2012; revised 23 Jul 2012; accepted 30 Jul 2012; published 1 Aug 2012

In this paper we report the first demonstration of an on-chip tunable, narrowband microwave photonic filter with a high Q. We also demonstrate that the shape and bandwidth of such a filter can be easily reconfigured. In this work we exploited the large SBS gain coefficient (g_B ~0.74 x 10^{-9} m/W) [23, 24] and small effective mode area (~2.3 μm^2) of an As_2S_3 rib waveguide to achieve large SBS gain in a 6.5 cm long rib waveguide at moderate pump power (~300mW). Our device provided a narrow 3dB bandwidth f_{3dB} ~23 ± 2MHz with stable amplitude ~20 ± 2 dB over a wide frequency range (2-12 GHz) resulting in a Q ~520: 52 times the Q values previously reported for on-chip MPFs [21]. The shape factor (S) of the MPF, which is defined as the ratio of −20 dB to −3 dB bandwidth, was also tuned from 3.5 to 2 by tailoring the pump profile [13, 25]. This demonstration represents a significant advance in the field of integrated microwave photonics.

2. Principle of operation

In this section we present the principle of operation of our microwave photonic filter. This principle was first demonstrated in [14] for the case of a long optical fiber. Here we review the basic operating principle, which is illustrated in Fig. 1, and also discuss some specific aspects that are unique to our device based on an As_2S_3 photonic chip.

In Fig. 1, a microwave signal A(Ω) is first encoded into an optical carrier (ω_o) using phase modulation. The phase encoding results in equal amplitude upper and lower sidebands that are out of phase by π. The beat signals between these out-of-phase sidebands and the carrier interfere destructively and, hence, no filtered signal appears in the microwave spectrum. However, when one of the side bands is amplified using SBS, the beat signals have different amplitudes and no longer cancel, resulting in the generation of a filtered signal in the microwave domain that has the spectrum and bandwidth of the SBS gain profile (see Fig. 1).

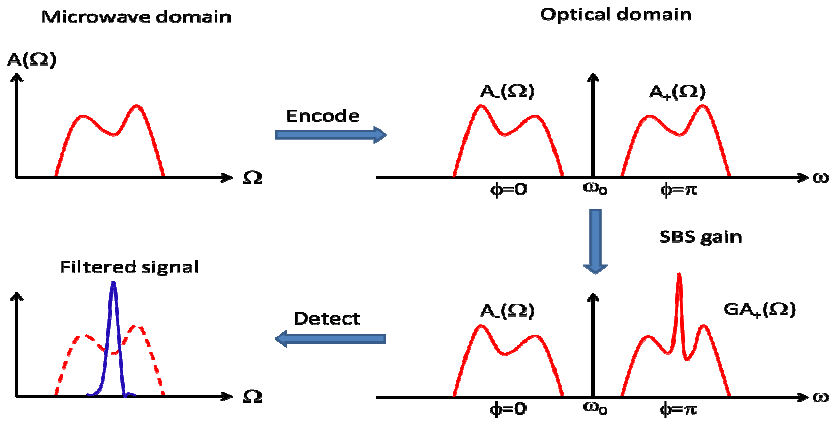

Fig. 1. Principle of stimulated Brillouin scattering based microwave photonic filter

The key to our photonic chip based microwave photonic filter (PCMPF) is the strong SBS cross-section (g_B) and small effective optical mode area (A_{eff}) of our chalcogenide (As_2S_3) waveguide [23, 24]. For SBS, the gain exponent $G = g_B P_p L_{eff}/A_{eff}$ depends on both g_B, and the pump intensity $I_p = P_P/A_{eff}$, where P_p is the pump power, and effective length L_{eff}. To achieve large SBS gain in a short device at moderate pump powers, therefore, requires a material with large g_B and a device with small A_{eff}. The gain coefficient g_B is enhanced using high refractive index materials, because g_B scales with n^8. Further enhancement can be achieved by ensuring that the photons and phonons are both guided within the same structure. An As_2S_3 chalcogenide glass waveguide satisfies these conditions [18] having a large refractive index n = 2.43 at 1550nm, which results in large g_B and also allows tight confinement of both the optical and acoustic modes in a rib waveguide structure. For our chalcogenide chip g_B ~0.74 x 10^{-9} m/W (~70 x silica) and A_{eff} = 2.3 μm^2, which results in large G at small pump powers.

#170558 - $15.00 USD Received 13 Jun 2012; revised 23 Jul 2012; accepted 30 Jul 2012; published 1 Aug 2012

3. Theory

Next we present a generalized theory of a MPF exploiting SBS and phase modulation of an optical carrier. The theory considers filtering of an arbitrary microwave signal A(Ω) instead of a sinusoidal signal and analyses the effect of any unwanted signals that may arise due to beating of the phase modulated signal with a co-propagating parasitic pump, introduced by the reflection at the lensed fiber-chip interface.

First we consider the ideal case of Fig. 1 where a microwave signal A(Ω) is phase encoded onto an optical carrier (ω_o) and filtered using SBS. After encoding, the resulting optical signal is given as:

$$E(t) = e^{j\omega_0 t} e^{j\phi(t)} = e^{j\omega_0 t}\left[1 + \int_{-\infty}^{\infty} A_{-}(\Omega) e^{-j\Omega t} d\Omega + \int_{-\infty}^{\infty} A_{+}(\Omega) e^{j\Omega t} d\Omega\right]. \quad (1)$$

Using the fact that for a phase modulated signal the intensity $I(t) = |E(t)|^2$ = constant, the contribution from non-DC terms must be zero. Assuming small-signal modulation and considering only the first order non-DC terms in I(t), we obtain:

$$\int_{-\infty}^{\infty}\left[A_{-}^{*}(\Omega) + A_{+}(\Omega)\right] e^{j\Omega t} d\Omega = 0, \quad (2)$$

which implies that for a phase modulated signal $A^*_{-}(\Omega) = -A_{+}(\Omega)$. This condition arises because no signal should appear on the radio frequency spectrum analyzer (RFSA) for a pure phase modulated signal.

When the SBS gain is applied to one of the phase modulated side bands (e.g. the upper sideband), the signal on the RFSA (assuming small-signal modulation) arises from the following non-DC terms:

$$I(t) \approx \int_{-\infty}^{\infty}\left[A_{-}^{*}(\Omega) + G(\Omega) A_{+}(\Omega)\right] e^{j\Omega t} d\Omega. \quad (3)$$

Using the fact that $A^*_{-}(\Omega) = -A_{+}(\Omega)$ in Eq. (3), the detected signal is given by:

$$I(t) \approx \int_{-\infty}^{\infty}\left(G(\Omega) - 1\right) A_{+}(\Omega) e^{j\Omega t} d\Omega. \quad (4)$$

From Eq. (4), it is evident that the output in the microwave domain has a spectrum $[G(\Omega)-1]A_{+}(\Omega)$ and thus, with respect to the input microwave signal A(Ω), the output microwave signal is filtered by the SBS gain response G(Ω)-1.The result in Eq. (4) shows that in the ideal case of Fig. 1, under the small-signal modulation approximation i.e. higher-order non-DC terms are neglected, the SBS process can be used to filter a microwave signal.

In our specific implementation that will be discussed in more detail below, due to the reflections at the ends of the chip, the injected counter-propagating pump generates a parasitic pump co-propagating with the phase modulated signal. Below we analyze the degradation of the filter response due to such a parasitic effect.

In order to analyze this non-ideal case, shown in Fig. 2, we rewrite Eq. (1) in the presence of a co-propagating backscattered pump with gain on the upper phase modulated sideband as:

$$E(t) = e^{j\omega_0 t}\left[1 + \int_{-\infty}^{\infty} A_{-}(\Omega) e^{-j\Omega t} d\Omega + \int_{-\infty}^{\infty} G(\Omega) A_{+}(\Omega) e^{j\Omega t} d\Omega + A_p e^{j(\omega_p - \omega_0)t}\right]. \quad (5)$$

#170558 - $15.00 USD Received 13 Jun 2012; revised 23 Jul 2012; accepted 30 Jul 2012; published 1 Aug 2012

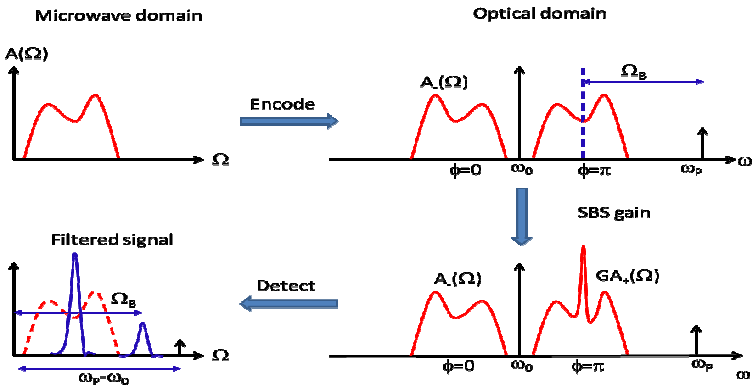

Fig. 2. Schematic of stimulated Brillouin scattering based microwave photonic filter with residual co-propagating pump which arises due to reflection at the lensed fiber and chip interface.

Once again assuming small-signal modulation and considering only the first-order non-DC terms in I(t), we obtain:

$$I(t) \approx \underbrace{\int_{-\infty}^{\infty} \left(G(\Omega)-1\right) A_{+}(\Omega) e^{j\Omega t} d\Omega}_{\text{Filtered Signal}} + \underbrace{\left[\begin{array}{c} A_p e^{j(\omega_p-\omega_0)t} + \int_{-\infty}^{\infty} A_p A_{-}^{*}(\Omega) e^{j(\omega_p-\omega_0+\Omega)t} d\Omega + \\ \int_{-\infty}^{\infty} A_p G^{*}(\Omega) A_{+}^{*}(\Omega) e^{j(\omega_p-\omega_0-\Omega)t} d\Omega \end{array} \right]}_{\text{Unwanted Signals}}. \quad (6)$$

The first term in Eq. (6) represents the filter operation as derived in Eq. (4). The remaining terms in Eq. (6) contribute to the degradation of the filter response by generating undesired signals. The second term arises from the beating between the carrier and residual pump and gives rise to a signal at ω_p - ω_0; the third term arises from the beating between the residual pump and unamplified sideband; and the final term results from beating between amplified sideband and the residual pump, which results in a microwave signal at the Brillouin shift Ω_B. In order to reduce these unwanted signals, we removed the parasitic pump signal at the output using a Bragg grating, however, there is still some residual pump which generates a small amount of unwanted beat signals. Furthermore, a small signal is generated from beating between the amplified and unamplified PM sideband. These unwanted terms, however, arise from practical constraints such as stray or scattered light from the pump, which can be eliminated by improving coupling into the rib waveguide using, for example, on-chip tapers.

4. Experiment

4.1 Set up

Figure 3 shows the experimental set up used to realize a PCMPF. Continuous wave (CW) light from a distributed feedback (DFB) laser was passed through an isolator and then split into two parts using a 99/1 coupler. The 1% port became the "pump arm" and was amplified using a 2W C-band EDFA (EDFA1) and passed through a polarization controller (PC1) before being launched into the chip via a circulator (C1) and a lensed fiber. The 99% port was used to generate a carrier suppressed intensity modulated signal using an intensity modulator (IM), which split the light into upper and lower sidebands. One of the IM sidebands was removed using a fiber Bragg grating (FBG1) before it entered a 90/10% coupler. The 90% port acted as the optical carrier on which the RF signal was encoded using a phase modulator (PM). The PM signal was then coupled into the chip via C2 and a lensed fiber. The

#170558 - $15.00 USD Received 13 Jun 2012; revised 23 Jul 2012; accepted 30 Jul 2012; published 1 Aug 2012

polarization of light going into the phase modulator and the chip was controlled using polarization controllers PC3 and PC5 respectively. The 10% arm was amplified using a low-noise EDFA (EDFA2), and passed through a polarization controller (PC4). The output of the chip was collected through circulator C1 and passed through FBG2, where the back-reflected pump due to reflections at the end faces of the chip was removed. The signal after pump removal was then coupled with the amplified carrier wave using a 50/50 coupler, one arm of which lead to an OSA and the other to a high-speed photo detector connected to a RFSA. The power of the re-injected amplified optical carrier was kept fixed throughout the experiment. The rib waveguide used in the experiments was 6.5 cm long with a cross-section of 4 µm x 850 nm with anti-reflection coatings applied to the end facets. The Brillouin shift of the chalcogenide (As_2S_3) chip is ~7.7 GHz.

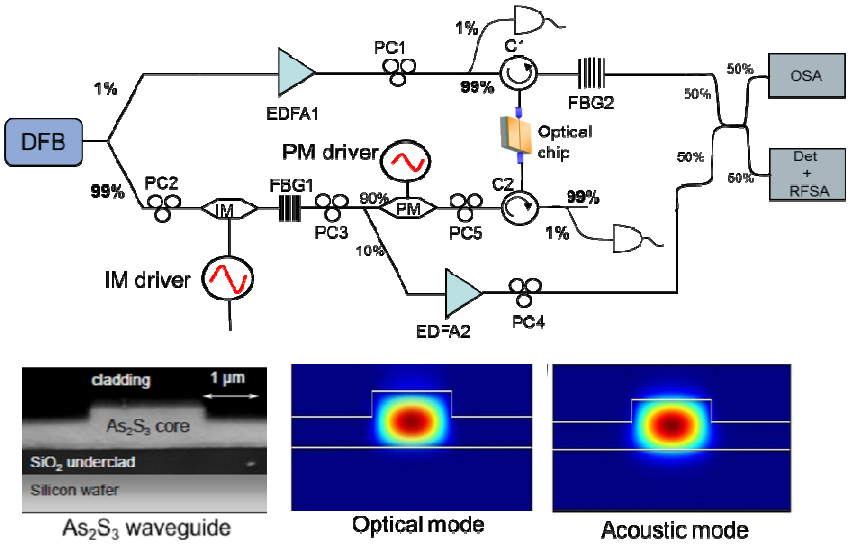

Fig. 3. Experimental setup to realize PCMPF using SBS along with the optical microscope image of a typical rib waveguide and optical and acoustic modes in the rib structure showing strong optical-acoustic confinement. PC: polarization controller, FBG: fiber Bragg grating, IM: intensity modulator, PM: phase modulator C: circulator, EDFA: erbium doped fiber amplifier, OSA: optical spectrum analyser, Det: photodetector and RFSA: radio frequency spectrum analyser.

4.2 General operation

In the experiment to demonstrate the PCMPF, the Brillouin pump frequency was kept fixed at the laser frequency (ω_L) while the frequency of the carrier, on which the RF signal (ω_{RF}) was phase encoded, was tuned using an intensity modulator (IM). The intensity modulator was biased to suppress the laser frequency as shown in Figs. 4(a) and 4(c). In the case when the RF frequency ω_{RF} was smaller than the frequency (ω_M) of the IM, the lower IM side band was used as the carrier while the upper IM sideband was removed using a tunable fiber Bragg grating (FBG1) as shown in Fig. 4(a). In this case, the upper phase modulated sideband experienced gain (see Fig. 4(b)). The parasitic pump, which originated from reflections at the interface of lens fiber and chip was removed using FBG2 (see Fig. 4(b)). The MPF center frequency (ω_{RF}) could be tuned in the range from 0 to $\omega^{max}_M - \Omega_B$, where ω^{max}_M is the maximum frequency determined by the IM and its driver. In our experiment the maximum frequency of the IM driver was ω^{max}_M = 15 GHz and therefore the MPF tuning range for this case i.e. when $\omega_M > \omega_{RF}$ was restricted from 0 to $\omega^{max}_M - \Omega_B$ ~7.2 GHz. In order to increase the tuning range beyond $\omega^{max}_M - \Omega_B$, we operated in a region where $\omega_M < \omega_{RF}$. Note that a single-sideband (SSB) IM and a signal generator with larger ω^{max}_M would provide much larger

#170558 - $15.00 USD Received 13 Jun 2012; revised 23 Jul 2012; accepted 30 Jul 2012; published 1 Aug 2012

tuning range without going into the $\omega_M < \omega_{RF}$ operating regime. This would also simplify the device operation by avoiding the need for FBG1.

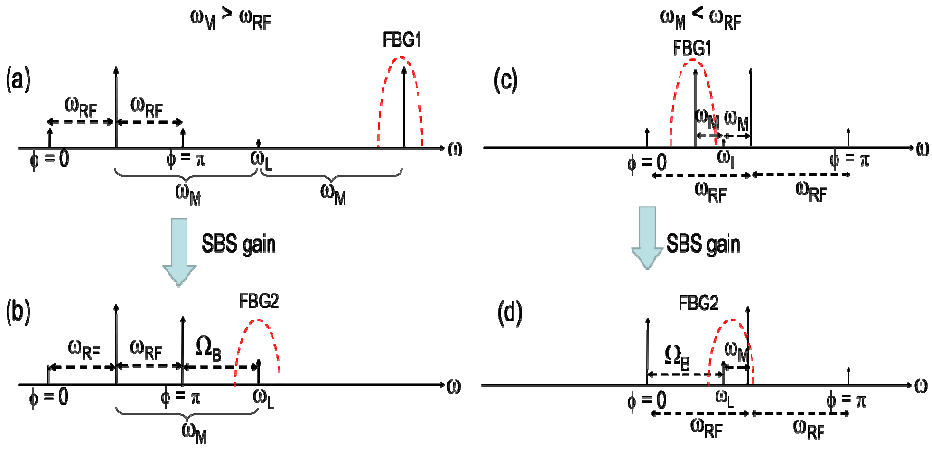

Fig. 4. Principle of general MPF operation when IM frequency greater than RF frequency $\omega_M > \omega_{RF}$ (a, b) and for IM frequency smaller than RF frequency $\omega_{RF} > \omega_M$ (c, d). For $\omega_M > \omega_{RF}$, lower IM sideband is used as a carrier for phase modulation and the upper phase modulated sideband experiences SBS gain. For $\omega_{RF} > \omega_M$, upper IM sideband acts as the carrier for phase modulation and lower phase modulated sideband experiences SBS gain. For $\omega_M > \omega_{RF}$, the IM carrier is blocked by FBG2, which was used to remove the parasitic pump.

When $\omega_M < \omega_{RF}$, the upper IM sideband acted as the optical carrier on which the RF signal was phase modulated while the lower IM sideband was removed using a FBG (see Fig. 4(c)). In this case, the lower PM sideband experienced gain (see Fig. 4(d)) and the MPF center frequency could be tuned from $\omega^{min}_M + \Omega_B$ to $\omega^{max}_M + \Omega_B$, where ω^{min}_M is the minimum frequency of the signal generator driving the IM. In our experiment, the maximum MPF tuning frequency was restricted to 12 GHz because both the phase modulator and its driver have a maximum range of 12 GHz. The lowest MPF center frequency in this operating regime ($\omega_M < \omega_{RF}$) was limited by the lowest frequency (ω^{min}_M) of the IM driver. The ω^{min}_M of 2 GHz restricted the lowest MPF frequency for this operating regime to ~10 GHz. Thus, the PCMPF could not be operated at 8 and 9 GHz in these experiments, however, this constraint is not a fundamental limitation of the system.

For both the operation regimes i.e. $\omega_M < \omega_{RF}$ and $\omega_M > \omega_{RF}$, the optical carrier wave was reintroduced after removing the residual back-reflected pump using FBG2. The reintroduced carrier makes up for the reduced carrier power after propagation through the chip where ~12 dB insertion loss was experienced by the phase modulated signal. The coupling to the chip was performed using lens-tip fibers with a spot size of 2.5 μm, which resulted in ~4dB coupling loss at each facet. For $\omega_M < \omega_{RF}$, the IM carrier was suppressed by the FBG2 (see Fig. 4(d)). A fixed carrier power was reintroduced for both the operating regimes before detection.

4.3 Filter tuning

Figure 5 shows the RFSA trace when a phase modulated (PM) signal centered at $\omega_{RF} = 7$ GHz counter-propagated with a pump such that the upper PM sideband was downshifted from the pump by Ω_B. In this condition the gain experienced by the upper PM sideband resulted in large amplitude mismatch between the two out-of-phase sidebands creating a large signal (~20 dB) on the RFSA at $\omega_{RF} = 7$ GHz. As predicted in the theory section, a small unwanted signal (~1.3dB) appeared at Ω_B (see inset Fig. 5), due to beating of the residual backscattered pump with the amplified PM sideband. Another small signal (~2.2 dB) appeared at $2\omega_{RF} = 14$ GHz, due to beating between the amplified and unamplified sidebands. The extinction measured in

#170558 - $15.00 USD Received 13 Jun 2012; revised 23 Jul 2012; accepted 30 Jul 2012; published 1 Aug 2012

comparison to the noise level is ~20 ± 2 dB. However, the unwanted beat signals, predicted by Eq. (6) and shown in the inset of Fig. 5 reduced the sideband suppression by ~3dB.

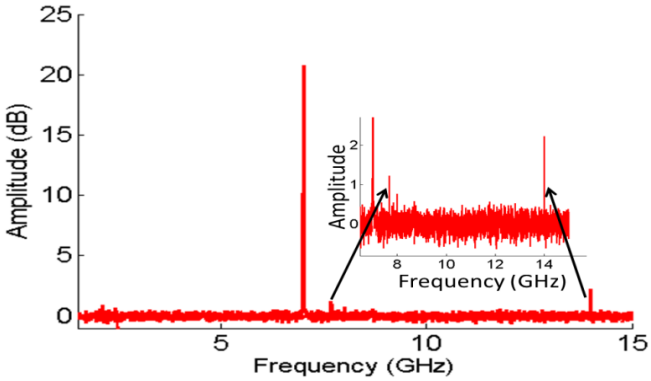

Fig. 5. RF trace for filtering of a phase modulated RF signal centered at ω_{RF} = 7 GHz using PCMPF showing a large signal ~20 dB on the RFSA at the RF frequency ω_{RF} = 7GHz and other small unwanted signals arising from the beating of residual co-propagating pump with amplified signal (Ω_B) and a signal arising from beating between the amplified and unamplified PM sideband at $2\omega_{RF}$ = 14 GHz (see inset).

With the pump off, a small signal (~4dB) appeared at ω_{RF} = 7GHz on the RFSA. We attributed this to imbalance between the power in the upper and lower PM sidebands due to asymmetry in the modulator and the presence of the grating (FBG2), which affected the sidebands differently. This resulted in incomplete cancellation of the out-of phase beat signals.

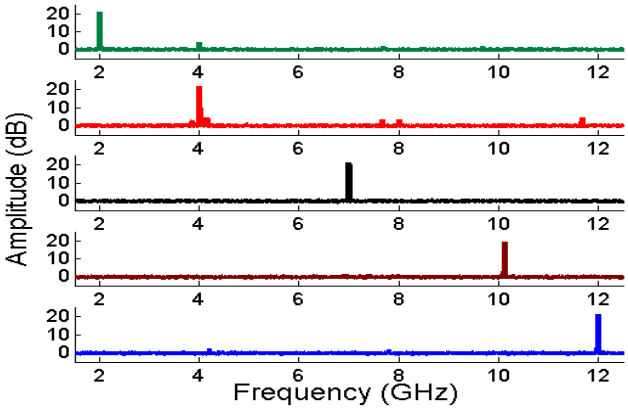

Fig. 6. Tuning response of the MPF centre frequency over the range 2-12 GHz demonstrating wide tuning range.

To tune the MPF center frequency, we tuned both the IM frequency and the PM driver frequency so that one PM sideband was always at the Brillouin shift from the pump. Figure 6 shows that the PCMPF could be tuned over a wide range (2-12GHz). A constant SBS gain of ~20dB was used to obtain Fig. 6. The amplitude and bandwidth fluctuations in the MPF response over the tuning range are shown in Fig. 7 demonstrating good amplitude (~20 ± 2 dB) and bandwidth (f_{3dB} ~23 ± 2 MHz) stability. The inset in Fig. 7 shows the MPF profiles centered at RF frequencies of 4 GHz and 11 GHz, obtained by scanning the PM driver frequency over 1 GHz. The maximum Q-factor, defined as the MPF center frequency divided by the f_{3dB}, was calculated to be ~520 for a RF center frequency of 12 GHz.

#170558 - $15.00 USD Received 13 Jun 2012; revised 23 Jul 2012; accepted 30 Jul 2012; published 1 Aug 2012

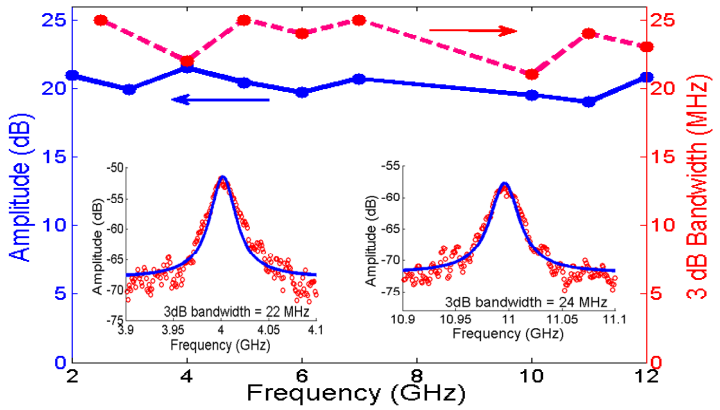

Fig. 7. Amplitude and 3dB bandwidth of PCMPF for different centre RF frequencies demonstrating good amplitude (~20 ± 2 dB) and bandwidth (23 ± 2 MHz) stability. Inset: MPF profiles taken at centre frequencies of 4 and 11 GHz.

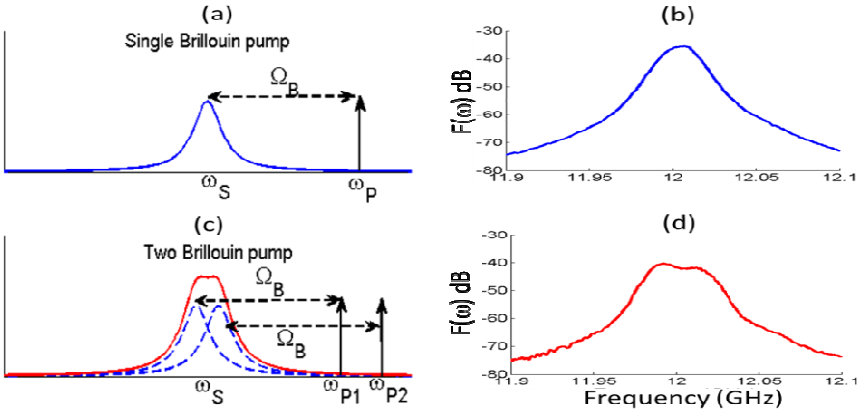

Fig. 8. Theoretical filter response for (a) single and (c) two pumps demonstrating MPF profile reshaping (flat top) with improved 3dB bandwidth. Measured MPF profiles for (b) single pump f_{3dB} ~20 MHz and (d) dual pump f_{3dB} ~40 MHz with shape factor improved from S = 3.5 (single pump) to S = 2 (dual pump). The reshaping results in flat topped filter profile.

To reconfigure the MPF 3dB bandwidth and shape factor, S, we tailored the pump profile [13, 25]. Figures 8(a) and 8(c) show that when we changed the pump spectrum from a single to dual-pump configuration the overall MPF profile (solid Fig. 8(c)), which results from the overlap of two individual gain profiles (dashed Fig. 8(c)), has a flat top and larger f_{3B}. Figures 8(b) and 8(d) show the measured PCMPF profiles for single and dual pumps (separated by 18 MHz), respectively. Using two pumps, a nearly flat-topped MPF profile was achieved with f_{3dB} increased from ~20 MHz to ~40 MHz, which in turn improved S from ~3.5 for a single pump to ~2 for the dual pump.

5. Conclusion

In conclusion, we have presented the first demonstration of a photonic chip based tunable, high Q, narrowband MPF with shape and f_{3dB} reconfiguration. A PCMPF with a stable 3dB bandwidth (~23 ± 2 MHz) and amplitude response (~20 ± 2 dB) over the tuning range of 2-12 GHz was demonstrated. The filter response was reconfigured by tailoring the pump profile, resulting in shape factor enhancement from 3.5 to 2 and f_{3dB} improvement from ~20 MHz to ~40 MHz. The sideband suppression was reduced due to unwanted signals arising from pump reflections. Improved coupling to the chip using, for example, inverse tapers would have

#170558 - $15.00 USD Received 13 Jun 2012; revised 23 Jul 2012; accepted 30 Jul 2012; published 1 Aug 2012

reduced facet reflections and increased the extinction ratio and sideband suppression substantially allowing a simpler experimental set-up by eliminating the need for FBG2. Further, use of a single-sideband intensity modulator with larger modulation frequency would increase the MPF tuning range and further simplify the experiment. This demonstration represents a significant advance in the field of integrated microwave photonics and enables the realization of potential applications in microwave signal processing for radar and analog communications.

Acknowledgments

This work was funded by the Australian Research Council (ARC) through its Discovery grant (DP1096838), Federation fellowship (FF0776056), and Center of Excellence CUDOS (Grant # CE110001018), and by the U.S. Department of Defense through AFOSR/AOARD (grant #FA23861114030).

#170558 - $15.00 USD Received 13 Jun 2012; revised 23 Jul 2012; accepted 30 Jul 2012; published 1 Aug 2012